Journal of Building Engineering 44 (2021) 103375

Contents lists available at ScienceDirect

Journal of Building Engineering

journal homepage: www.elsevier.com/locate/jobe

Innovative particleboard material from the organic fraction of municipal solid waste

Michael M. Santos [a,b,**], Maria A. Diez [a], Marta Suárez [c], Teresa A. Centeno [a,*]

[a] Instituto de Ciencia y Tecnología del Carbono (INCAR-CSIC), Francisco Pintado Fe 26, 33011, Oviedo, Spain
[b] Centre of Materials and Building Technologies (C–MADE/UBI), Department of Civil Engineering and Architecture, University of Beira Interior (UBI), 6201-001, Covilhã, Portugal
[c] Centro de Investigación en Nanomateriales y Nanotecnología (CINN-CSIC), Universidad de Oviedo (UO), Principado de Asturias (PA), Avda. de la Vega, 4-6, 33940, El Entrego, Spain

ARTICLE INFO

Keywords:
Food waste
Hydrothermal carbonization
Hydrochar
Building material
Particleboard

ABSTRACT

This study presents a challenging approach that addresses the efficient management of the organic fraction of municipal solid waste (OFMSW) by hydrothermal carbonization (HTC) for the development of novel sustainable low-CO_2 building materials. Mild HTC treatment at 180 °C for 2 h transformed low-grade OFMSW into a renewable carbonaceous solid (hydrochar), which displays promising properties for application in particleboards. Taking advantage of the presence of extractives acting as natural binders, the hydrochar particles with sizes of <0.3 mm, 0.3–1 mm, and 1–2 mm agglomerate successfully by simple pressing at 3 MPa for 7 min at room temperature (~ 25 °C). The resulting binderless monolithic probes display a density of 838 and 883 kg/m^3 for the finest and coarsest grain sizes, respectively, and approximately 30% porosity. The mechanical resistance is enhanced by the use of larger particle sizes, and values of modulus of rupture and tensile strength of 21.64 MPa and 18.99 MPa are reached, respectively. The thermal conductivity of the probes in the range of 0.091–0.132 W/(m•K) suggests the potential of OFMSW-derived hydrochar for thermal insulation panels.

1. Introduction

The urgent need to minimize CO_2 emissions generated by the construction sector has prompted efforts to include waste or by-products from various industrial activities as a partial substitute for the raw materials currently used [1–5]. This approach not only mitigates the intensive exploitation of primary resources, but also enables the simultaneous sustainable disposal of residues massively generated daily.

Despite its promising potential, biomass waste still presents a number of drawbacks for direct application in the construction materials industry, mainly derived from the humidity content, low mechanical properties, and poor compatibility with other components [6,7]. The advantages of the biomass-based composites over conventional materials, such as a more competitive cost, low amount of CO_2 gas emissions, low densities, and relatively good thermal and acoustic insulation, cannot obviate that the presence of biomass implies important detrimental effects [6]. Several studies have raised concerns about its limited durability in the alkaline cement matrix and the delay of cement hydration due to the presence of hemicellulose as a source of sugars. Furthermore, high water absorption and poor cement-biomass compatibility negatively affect the mechanical properties and durability of the final product [2,3].

Particleboards made from biomass waste associated with wood offer promising prospects for the development of more competitive panels. It has been found that several residues, such as rice husks, coffee husks, sugar cane bagasse, grape bagasse, carpels of macadamia nuts, and papaya stalks, may be viable alternatives for partial or full replacement of wood in panels [8–11]. The results obtained in past studies largely depend on the biomass material used, the percentage of wood and the manufacture procedure. These factors widely influence the mechanical properties and water absorption of the final products.

Among the various options already studied to improve the properties of biomass for construction practices, the so-called biochar, the solid product from the thermochemical transformation of biomass, is

* Corresponding author.
** Corresponding author. Centre of Materials and Building Technologies (C–MADE/UBI), Department of Civil Engineering and Architecture, University of Beira Interior (UBI), 6201-001 Covilhã, Portugal.
E-mail addresses: michael.santos@ubi.pt (M.M. Santos), teresa.centeno@csic.es (T.A. Centeno).

https://doi.org/10.1016/j.jobe.2021.103375
Received 27 July 2021; Received in revised form 17 September 2021; Accepted 23 September 2021
Available online 27 September 2021

receiving great interest as an efficient replacement in cement and lightweight aggregates for ecological building materials [3,12–16]. Biochar production involves the thermal treatment of the precursor in an oxygen-free atmosphere. The most widely used temperatures range between 300 °C and 650 °C. Nevertheless, depending on the feedstock and the characteristics required for final applications of the biochar, the synthesis temperature can reach 900-1000 °C. Furthermore, other operating variables, such as heating rate and residence time at maximum temperature, play a relevant role and a wide variety of materials can be obtained for diverse applications [17,18]. However, this technology still faces the generation of polluting liquids and greenhouse gas emissions, and its efficiency is severely penalized by the high moisture content of most biomass wastes [19].

In this context, hydrothermal carbonization (HTC) has emerged as a sustainable process, whose strength relies precisely on the thermochemical transformation of wet feedstocks without the pre-drying step required for traditional biochar production. Moreover, being carried out at mild temperatures of 180–250 °C under autogenous vapor pressure, HTC presents a more affordable technical applicability and lowers the production time and cost [17,19–22]. The hydrothermal degradation of biomass follows reaction mechanisms similar to those in biochar production (hydrolysis, dehydration, decarboxylation, aromatization and recondensation) [19,23–26]. However, under HTC conditions, the process requires a lower activation energy as it is initiated by hydrolysis, and the high ions concentration derived from the decrease in the dielectric constant of water favours the decomposition of biopolymers and solubilisation of organic compounds [27]. In comparison to the biochar production, hydrothermal carbonization requires much less energy and generates higher yield of solid and water-soluble organic compounds, while gas generation does not usually exceed 5 wt%.

Disposal of the huge urban solid waste (MSW) streams generated daily worldwide is managed mainly through incineration and landfilling, which represent a major environmental concern. Currently, the recycling of the organic fraction of MSW is based almost exclusively on composting and anaerobic digestion and its potential as a sustainable resource is not yet fully exploited.

Different studies have shown that HTC successfully converts food waste into a carbon-enriched solid (hydrochar) and an aqueous phase [23–26]. Pathogens and organic contaminants are eradicated, while both by-products are used for energy production and storage, carbon sequestration, soil amelioration, adsorbents, catalysis, and chemicals and nutrients recovery [19–23].

This study addresses a challenging approach focused on the use of hydrochar derived from the organic fraction of municipal solid waste as an eco-innovative solution for sustainable particleboards. The results show that this novel application for hydrochars should be further investigated.

2. Materials and methods

2.1. Materials

2.1.1. Organic fraction of municipal solid waste (OFMSW)

The material used as feedstock was food waste collected separately from households. It mainly consisted of 66 wt% fruit and vegetable residues (orange, grapefruit, lemon, kiwi, strawberry, pineapple, onion, leek, garlic, cauliflower, broccoli, etc.), 20 wt% bread, pasta and rice, 6 wt% meat and fish waste (including bones), 3% eggshells, and 3% coffee grounds.

Proximate and ultimate analyses as well as calorific value determination were accomplished. Moisture and ash content were evaluated following the standard ASTM D7582–15 [28], whereas the percentage of volatile matter was assessed according to ISO18123 [29]. The ash-free carbon-rich solid remaining after drying and devolatilization (fixed carbon, FC) was calculated by subtracting the percentages of moisture, ash, and volatile matter from 100%. The elemental analysis was accomplished by dry combustion in a LECO TruSpec Micro analyser for C, H, N, and S, and oxygen was estimated by the difference from the mass balance. The higher heating value (HHV) was evaluated using an IKAWEEME C4000 adiabatic bomb calorimeter.

2.1.2. Hydrochar

A representative sample of OFMSW was subjected to hydrothermal treatment in a 3-L stainless-steel lined pressure reactor ILSHIN at 180 °C for 2 h, under the respective water vapor saturation pressure of 9 bar. The solid-to-water ratio was 1:4 by weight, including the moisture content of the feedstock (57 wt%) in the calculation of the water amount. Based on the reaction temperature (T (°C)) and time (t (minutes)), the severity of the process corresponds to log Ro = 4.43 (Eq. (1)), suiting a standard HTC treatment under mild conditions [30].

$$Ro = t \times \exp\left[\frac{T-100}{14.75}\right] \quad (1)$$

The solid product (hydrochar) was separated from the reaction aqueous phase by gravity filtration and washed with 1.5 L of water to drag the remains deposited on the surface. Finally, it was air-dried in an oven at 105 °C for 24 h.

The percentage of hydrochar (Y) obtained with respect to the mass of dry OFMSW was determined by Eq. 2

$$Y\,(\%) = \frac{mass\ of\ dry\ hydrochar}{mass\ of\ dry\ feedstock} \times 100 \quad (2)$$

Hydrochar chemical features and calorific value were evaluated by using the same protocol and standards [28,29] outlined above for the OFMSW characterization.

To assess the ratio of soluble to insoluble fractions in the hydrochar, a powdered sample (0.5 g) was immersed in distillated water (25 mL) and the mixture was heated at a constant temperature of 40 °C and continuously sonicated for 1 h. The suspension was cooled to room temperature and then filtered under vacuum through ashless filter paper (17 μm pore size) to separate the extract from the solid by-product. The latter was dried at 70 °C until no change in weight was detected.

Energy densification ratio (E_d), energy yield (E_y), and carbon recovery in hydrochar (C_{rec}) were evaluated as follows:

$$E_d = \frac{HHV_{hydrochar}}{HHV_{feedstock}} \quad (3)$$

$$E_y(\%) = E_d \times Y \quad (4)$$

$$C_{rec}(\%) = \frac{\%C_{hydrochar}}{\%C_{feedstock}} \times Y \quad (5)$$

where % $C_{hydrochar}$ and % $C_{feedstock}$ correspond to the carbon percentage in the hydrochar and the OFMSW, respectively.

2.1.3. Hydrochar probes

The hydrochar was crushed and sieved to select size dust and fine fractions of <0.3 mm, 0.3–1 mm, and 1–2 mm. Grain sizes were selected on the basis of those used in several studies [31–33], and taking into account the limitation imposed by mould dimensions to use larger particles. Monoliths in cylindrical shapes were prepared by mixing 4 g of hydrochar (0.43 wt% moisture) with 10 wt% of water relative to the hydrochar mass. The mixing process was carried out manually for approximately 1 min at laboratory temperature (~25 °C).

By using steel cylinder-shaped molds and applying an uniaxial pressure of 3 MPa for 7 min in a static hydraulic press, probes of 12.5 in diameter and different thicknesses were produced at ~25 °C for each of the above particle size fractions for subsequent analysis. The resulting samples are denoted by P, followed by 03, 031, and 12, according to the particle size used (Fig. 1). Sample dimensions are reported below.

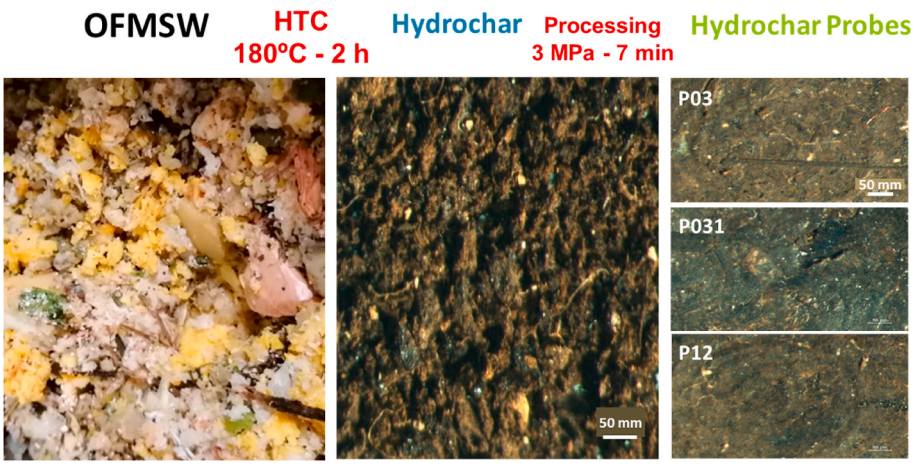

Fig. 1. Images of feedstock, hydrochar, and the surface of the probes obtained by compacting hydrochar particles of <0.3 mm, 0.3–1 mm and 1–2 mm in size.

2.2. Methods

Following the same procedure described in section 2.1.3, probes were prepared with the required length/diameter ratio for the different analytical techniques. To obtain the most accurate volume, thickness and diameter dimensions were measured using a calliper. All probes were air cured at 50 °C for 12 h prior to subsequent analysis.

2.2.1. Thermogravimetric analysis

Small items of 10 mm in diameter and about 1 mm in height were prepared for thermogravimetric analysis. The diameter was suited to the size of the crucible that served as sample container and thickness was chosen to minimize temperature gradient in the probe.

Pyrolysis and combustion experiments were carried out in a high-capacity thermoanalyser (METTLER TG-DSC1 Star system). Each monolith (100 ± 10 mg) was placed in an open platinum crucible (900 μL) and heated at a constant rate of 20 °C/min from 30 °C to 1000 °C with a holding time of 5 min. Nitrogen at a flow rate of 75 mL/min was used as an inert gas to sweep out the volatile products, while air (75 mL/min) was used as an oxidizing gas for combustion.

The following parameters were obtained from the pyrolysis tests:

VM_T: the amount of volatile matter evolved up to a specific temperature (T)
CY_{1000}: char yield at 1000 °C
DTG_{max}: the maximum mass loss rate
DTG_{mean}: the average mass loss rate
T_{max}: the temperature at which DTG_{max} occurred

whereas the analysis of the combustion profiles reported:

X: conversion expressed as per cent is the reacted part of the dry initial sample
X_T: conversion at a specific temperature (T)
$T_{ignition}$ and $T_{burnout}$: the temperature at conversion reaches 2% and 98%, respectively
Combustibility range: $T_{burnout}$ - $T_{ignition}$
R_w: combustion stability index [34,35].

$$Rw = \frac{DTG\max \times DTGmean}{Tignition^2 \times Tburnout} \quad (6)$$

2.2.2. Temperature-programmed desorption

CO_2 and CO evolved from the surface of P031 probe were studied by Temperature-Programmed-Desorption (TPD) from 20 °C to 1000 °C at 15 °C/min under 50 mL/min argon flow (Setaram TGA92 coupled to mass spectrometer OmnistarTM-Pfeiffer Vacuum).

2.2.3. Porous structure

The porous network of the powdered hydrochar and the derived probes was characterized by mercury porosimetry (Micromeritics AutoPore IV 9500) by applying pressures from 0.005 MPa to 228 MPa.

The N_2 adsorption isotherm at 77 K (Micromeritics ASAP 2010) of the powdered hydrochar was used to confirm the absence of narrow pores. Details of these techniques are summarized in the appendix.

2.2.4. Mechanical properties

Uniaxial compression testing was conducted to investigate the mechanical characteristics of the hydrochar probes using a universal mechanical testing machine (Instron Model 8562). Circular prisms of 12.5 mm diameter and 6.5 mm height were fixed on the testing platen. The compression strength was determined from the maximum load of the stress-strain curve obtained from the load-displacement measurements using a 10 kN load cell at a strain rate of 1.7 mm/s. The stress (σ) was evaluated by using Eq. (7):

$$\sigma = \frac{F}{A} \quad (7)$$

where F (N) is the load under the compressive test, and A (mm^2) corresponds to the sample section. Three probes were tested for each experimental condition. The average value and standard deviation are reported below.

The modulus of rupture was determined under the same conditions by applying a bending load concentrated in the center with a span of 15 times the thickness of the sample. It was calculated by load-deflection curves.

The tensile strength (Tp) of the hydrochar probes was estimated by Eq. (8) [36].

$$Tp = \frac{2f}{\pi l d} \quad (8)$$

where f (N) corresponds to the maximum force, and d (mm) and l (mm) are the diameter and length of the samples, respectively.

Each sample was placed between the two anvils of the universal mechanical testing machine (Instron Model 8562). A compressive force (10 kN, 1.7 mm/s) was applied until sample deformation.

2.2.5. Water absorption and thickness swelling

Prior to determinations, the samples (12.5 mm in diameter and 7.5–8.0 mm in thickness) were conditioned at (20 ± 2) °C until the results of two consecutive weightings, within a 24-h interval, did not differ by more than 0.1%.

To evaluate the hydrophobicity, the hydrochar probes were immersed in water at (20 ± 1) °C for 2 h, and the water absorption (A,

%) was determined following Eq. (9):

$$A = \frac{m_2 - m_1}{m_1} \times 100 \quad (9)$$

where m_1 and m_2 correspond to the mass (g) of the dry and wet samples, respectively.

Following UNE-EN317:1994 [37], the swelling in thickness (TS, %) was estimated by using the following equation:

$$TS = \frac{hf - hi}{hi} \times 100 \quad (10)$$

where hi and h_f are the initial and final thickness (mm) at the equilibrium of the probes, respectively.

2.2.6. Thermal insulation properties and bulk density

Thermal conductivity (λ) was estimated following Eq. (11):

$$\lambda = a \times \rho \times Cp \quad (11)$$

where λ is expressed in W/(m•K); a, ρ and Cp correspond, respectively, to the thermal diffusivity (m^2/s), the density (g/m^3) and the specific heat capacity (J/(g•K)) at 25 °C.

The thermal diffusivity of the monolithic probes (12.5 mm in diameter and 6.5–8.0 mm in thickness) was determined in a NETZSCH LFA 457 MicroFlash [38] and the bulk density was estimated from the ratio of the mass to the volume of individual probe [39]. The specific heat capacity was assessed in continuous mode using a heating ramp of 0.1 °C/min from 20 °C to 40 °C and 2 h of stabilization at the initial and final temperatures. This was accomplished using a C80 calorimeter (Setaram Instrumentation), and data analysis was carried out by Calisto software. To ensure reproducibility and consistency, three replicates were measured for each set of samples.

3. Results and discussion

3.1. Conversion of OFMSW by HTC

Although the characteristics of the organic fraction of municipal solid waste are highly dependent on regional, seasonal and socio-economic issues, the OFMSW used in this study have a similar elemental composition to those from Greek and Italian cities [40]. As shown in Table 1, OFMSW is mainly composed of carbon and oxygen with contents of around 40% by weight (dry basis). Moisture content depends on the different way of collection and management of this type of waste in each municipality. In the present OFMSW, moisture is 57% by weight (Table 1).

Avoiding previous energy consumption for drying, hydrothermal treatment at 180 °C for only 2 h minimises the high polluting impact of wet OFMSW by transforming it into a stable and partially carbonised material (Fig. 1). A yield of 30 wt% and a carbon recovery of 44 wt% with respect to the initial residue (dry basis) are obtained.

The inorganic fraction in the hydrochar (ash) represents nearly 12 wt % and is dominated by the macroelements Ca, Mg, P, S, and alkalies, among other minor components such as Fe, Zn, Mn, and Cu (Table 2).

When the ash content of hydrochar is calculated from that of the precursor OFMSW (12.9 wt%) and the hydrochar yield (30 wt%), about 40 wt% of mineral species should be distributed in the hydrochar. However, the experimentally determined ash content is significantly lower than the estimated value (12.2 wt% *vs*. 40 wt%) and similar to that of the OFMSW, which is indicative that a large part of the inorganics are moved to the liquid phase via solubilisation of some mineral species under HTC conditions.

Table 2
Presence of inorganic elements in the OFMSW derived-hydrochar.

Ca (% CaO)	7.87
P (% P_2O_5)	0.853
S (% SO_3)	0.532
Mg (% MgO)	0.211
K (% K_2O)	0.181
Na (% Na_2O)	0.133
Cl^- (%)	<0.130
Fe (mg/kg)	649
Zn (mg/kg)	49.3
Mn (mg/kg)	21.8
Cu (mg/kg)	14.5
B (mg/kg)	9.15
Ni (mg/kg)	7.86
Pb (mg/kg)	1.61
Mo (mg/kg)	0.675
Cr (mg/kg)	<2.00
Cd (mg/kg)	<0.100
Hg (mg/kg)	<0.100

The significant decrease in oxygen by approximately 55.6% and the increase in fixed carbon up to a value of more than double of the original OFMSW indicates the removal of low-molecular-weight compounds. The successful carbonization of OFMSW by hydrothermal treatment is also confirmed by an atomic O/C ratio of 0.23 for the resulting solid, which is a value that fits into the range of lignites with an O/C ratio of nearly 0.28 [41]. Nevertheless, the higher H/C (1.69) reveals that the hydrochar displays a lower evolution degree than coal [42].

HTC process applied to OFMSW produces an energy densification ratio, E_d, of 1.44 and a solid CO_2 neutral fuel with a calorific value of 21.5 MJ/kg is obtained. The attainment of 30% of hydrochar in relation to the mass of the starting material leads to an energy yield of 43%, which favorably competes with E_y = 27-24% achieved by more severe HTC of OFMSW at 220–260 °C and 60–250 min [43].

3.2. Pyrolysis and combustion behavior

Fig. 2 summarizes the DTG profiles obtained from pyrolysis (a and c) and combustion (b and d) tests carry out with OFMSW, the hydrochar and the corresponding probes with different particle dimensions.

The DTG curves of the pyrolysis of powered OFMSW and hydrochar (Fig. 2a) clearly show significant changes in the thermal events of volatile matter evolution (the maximum evolution rate and temperature interval) because of HTC.

The first common DTG variation from 30 °C to 150 °C is assigned to moisture release (event I). It is followed by a main decomposition stage of the components up to nearly 600 °C (event II), which is attributed to the degradation of structural and non-structural organic components present in the bio-organic fraction of OFMSW and the formation of char. The weight loss decreases in this pyrolysis stage from 65 wt% to nearly 47 wt% for OFMSW and hydrochar, respectively (Table 3), and it may be associated with the breakdown and solubilisation of polysaccharide molecules and other biomolecules during HTC. As a result, the pyrolysis DTG profile of hydrochar (event II) conforms to the typical profiles of lignocellulosic biomass with three distinct steps [44]. Cellulose exhibits the maximum degradation rate (5.78%/min) at a T_{max} of 368 °C.

Table 1
Chemical features and calorific value of the OFMSW and the corresponding hydrochar (referred to dry basis).

Sample	Moisture (%)	Ash (wt%)	VM (wt%)	FC (wt%)	C (wt%)	H (wt%)	N (wt%)	S (wt%)	O (wt%)	HHV (MJ/kg)
OFMSW	57.0	12.9	74.3	12.8	39.8	5.1	1.6	0.1	40.5	14.9
Hydrochar	0.43	12.2	61.0	26.8	59.0	8.3	2.4	0.1	18.0	21.5

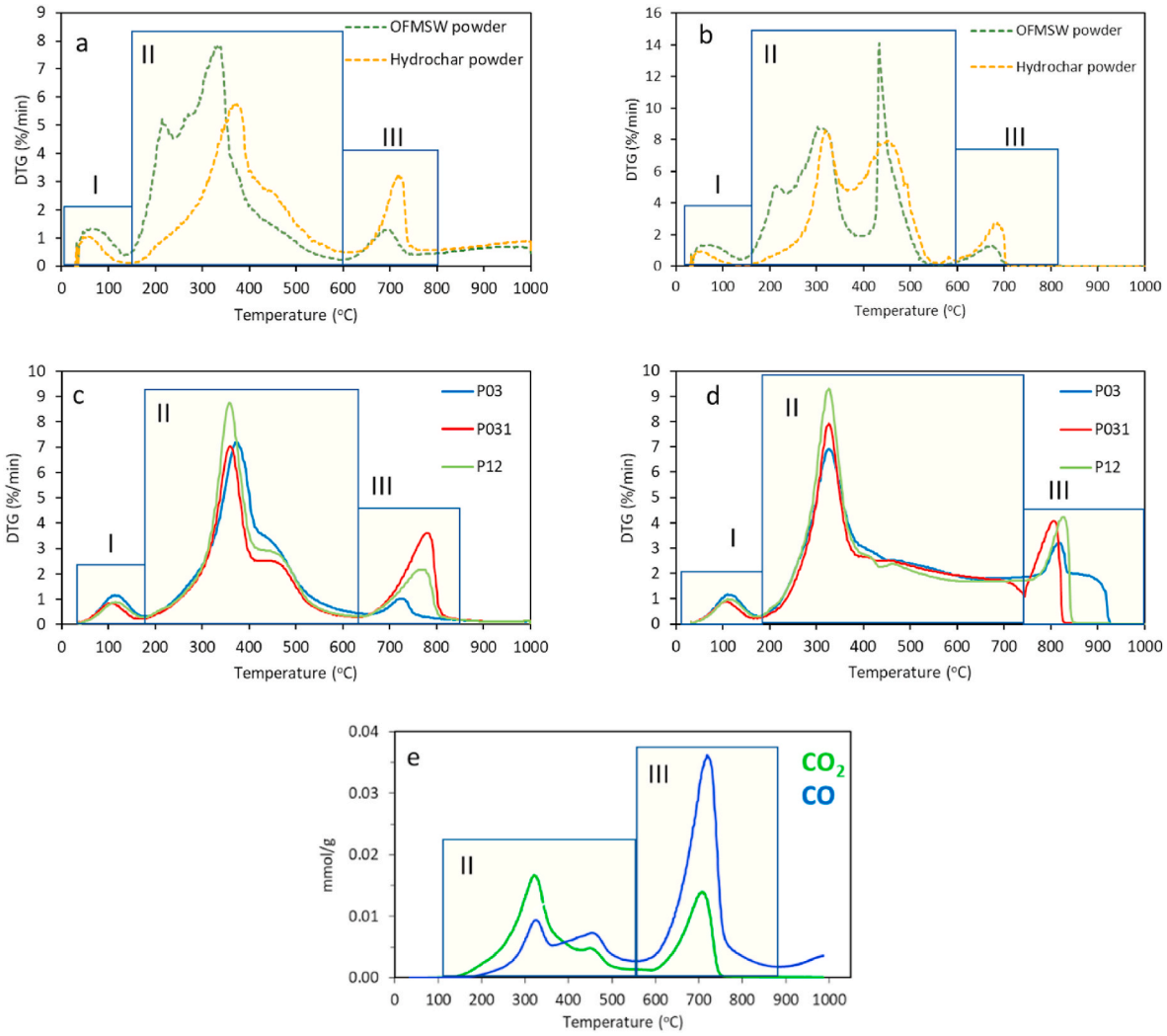

Fig. 2. DTG curves of OFMSW, the hydrochar and the corresponding probes prepared with hydrochar at different particle sizes during: (a and c) pyrolysis; (b and d) combustion, and TPD profile for the probe P031 (e).

Hydrochar does not show the well-defined low-temperature shoulder of hemicellulose (front of the main peak in Fig. 2a) present in the OFMSW profile, probably due to the partial removal of hemicellulose and more thermally unstable extractive biomolecules by HTC. Lignin occurs in hydrochar together with the two components based on polysaccharides. It decomposes with a maximum rate of 3.78%/min at around 400 °C (shoulder of the main peak in Fig. 2a). Whereas hemicellulose and cellulose exhibit a high decomposition rate over a narrow temperature range, lignin pyrolysis starts at about 200 °C and ends at 650 °C [44].

In addition to the elimination of the most thermally unstable components in the hydrochar, it is observed that their decomposition causes a shift of the degradation of the remaining bio-components towards higher temperatures. In the case of the cellulose, T_{max} is displaced from 335 °C to 368 °C. Likewise, the thermal transformation of the resulting char and some mineral species occur at higher temperatures (702 °C *vs*. 720 °C (event III)). This finding is coherent with the removal of a portion of the native inorganics with catalytic action in pyrolysis that are transferred to the aqueous phase (Table 1).

The pyrolytic behavior of the probes with hydrochars of different sizes resembles that observed for raw hydrochar (Fig. 2a and c). In general, the pressing of the hydrochar particles delays the water release from the probes for nearly 20 °C, the volatile evolution of the more thermally unstable components in the temperature range between 200 °C and 600 °C, and the hydrochar transformation from 600 °C up to 750–850 °C. The latter is more remarkable for medium- and coarse-particle grains. The densification of the hydrochar also enhances the formation of high-temperature char (CY_{1000}).

The hydrochar in powder or densified still contains a high quantity of oxygen-containing functionalities, as revealed by the CO_2 and CO desorption profiles obtained by TPD experiments (Fig. 2e). The surface oxygen content of around 9.15 mmol/g found for P031 is mostly distributed in several oxygenated functionalities with acidic and basic character such as carboxylic, lactones, α-substituted ketones and/or aldehydes, anhydrides, and phenolic groups [45,46]. They start to desorb at 150 °C and 200 °C (as CO_2 and CO, respectively), and the overlapping evolution of CO_2 and CO mostly occurs in the two events taking place at ranges of 200–550 °C (event II) and 600–800 °C (event III). The release at low temperature is more concentrated in CO_2 due to the presence of weak carboxylic groups; the phenolic-type functionalities are responsible for the clear dominance of CO evolution at high temperatures.

As in the pyrolysis process, the combustion of OFMSW and the hydrochar in powder and densified occurs at three stages (Fig. 2b and d): dehydration (event I), simultaneous transformations related to the formation of char and the combustion of volatiles and resultant char (200–550 °C, and prolonged up to 750 °C for the compacted hydrochar particles), and combustion/burnout of the remaining char and transformation of some minerals into ashes. In the combustion of densified hydrochars, the most notable differences are the prolongation and

Table 3
Pyrolysis and combustion behaviour of OFMSW, the hydrochar in powder and the hydrochar probes.

	OFMSW powder	Hydrochar powder	Hydrochar probes		
			P03	P031	P12
Pyrolysis behaviour					
Moisture (wt%)	5.4	3.0	4.0	2.9	3.1
VM_{250} (wt% db)	16.2	3.4	2.6	2.2	2.5
VM_{400} (wt% db)	55.7	30.4	32.1	29.2	34.7
VM_{600} (wt% db)	65.0	47.1	52.7	44.4	52.2
VM_{750} (wt% db)	70.5	57.3	57.2	51.3	58.1
VM_{1000} (wt% db)	80.5	70.1	59.8	61.4	64.6
CY_{1000} (wt% db)	19.5	29.9	40.2	38.6	35.4
T_{max} (°C)	335	368	375	364	359
DTG_{max} (%/min)	7.857	5.776	7.186	7.043	8.753
Combustion behaviour					
Moisture (wt%)	5.3	2.4	4.4	3.9	3.6
X_{250} (%)	18	3	3	3	4
X_{400} (%)	63	44	35	38	42
X_{600} (%)	95	91	64	68	69
X_{750} (%)	100	100	74	87	84
X_{1000} (%)	100	100	100	100	100
$T_{ignition}$ at X = 2% (°C)	175	225	226	233	233
$T_{burnout}$ at X = 98% (°C)	670	686	899	805	834
Combustibility range (°C)	495	461	673	572	611
R_w x 10^7	3.3	1.8	1.3	1.1	1.2

continuity of thermal event II from 400 °C to almost 750 °C together with the transformations that occur at the highest temperature. The DTG curves indicate a similar combustibility of the probes with an ignition temperature of around 230 °C at 2% conversion degree and a lower combustion stability index (R_w) of 1.1–1.3, compared to that of OFMSW and the resulting hydrochar (3.3 and 1.8, respectively). Another remarkable difference is the broadening of the combustibility range between the ignition and burnout due to an increase in the burnout temperature of the samples.

3.3. Porous structure

Regarding to the porous structure, whereas N_2 adsorption indicates poor development of narrow pores in the hydrochar with a specific surface area (S_{BET}) of 12 m^2/g (see Fig. A1 in the Appendix), mercury porosimetry reveals that the porous network is made of a broad pore size distribution (PSD) ranging from 0.1 to 27 μm (Fig. 3). The cumulative pore volume (Fig. 3a) and the pore size distribution (Fig. 3b) reveal that part of that porosity (mostly >2 μm) is lost during processing under pressure and the initial porosity of 60% in the range 5.5 nm–12 μm is reduced to a value of around 30% in the manufactured samples. Fig. 3 illustrates that the pore size distribution in the probes is highly dependent on the particle size. In the case of using particles smaller than 0.3 mm, the pores are concentrated in the range 0.2–4 μm, but the presence of wider pores becomes significant as larger particles are agglomerated. Thus, the maximum observed with smaller particles disappears and PSD widens to 15 μm and 250 μm when processing particles of 0.3–1 and 1–2 mm, respectively.

The different porous structure of the agglomerated samples is not reflected in their bulk density, ranging from 838 kg/m^3 for P03 and P031 with the smaller particles to 883 kg/m^3 for the coarsest grain sizes (P12) (Table 4). These values classify the hydrochar-probes as of high density [47].

It should be noted that OFMSW-hydrochar probes are slightly denser than pellets of torrefied wood (805.5 kg/m^3) prepared under much more severe compacting conditions [48] and quite comparable with particleboards based on palm tree prunings (819–856 kg/m^3) and Washingtonia palm rachis (779–812 kg/m^3) agglomerated with resin and citric acid.

3.4. Mechanical properties

Currently, particleboards have a wide variety of end uses, such as building materials, structural components, decorative cladding and joinery, etc., and therefore high mechanical strength is a key feature for their successful implementation.

Extensive research is underway to determine the role of the particle dimensions on the mechanical properties, although no general patterns have been obtained so far. Such a difficulty reflects that particleboard durability also depends on the physicochemical features of the raw materials, adhesive type and amount, additives, press conditions, moisture content and temperature [8,53].

The present hydrochar probes reach values of modulus of rupture (MOR) between 14.44 and 21.64 MPa (Fig. 4), which comply with the minimum value of 10.5 MPa established by the European standard for general use of wood-based panels [52]. The particle size is a relevant parameter as far as a clear improvement in the compressive strength of the probes with larger particles is observed (Fig. 4). This enhancement is not consistent with the increased strength reported for panels made of plant fibers as particle size decreases [54–56]. On the contrary, it does agree with the higher modulus of rupture displayed by hybrid grapevine/pine panels when larger grapevine particles (1.00–2.35 mm) were used. The diverging data summarized in Table 4 indicate the need for systematic studies accomplished under standard procedures of manufacturing and testing to get clear correlations between both parameters.

It should be noted the promising behavior of the present OFMSW-hydrochar probes, in terms of MOR. It is shown in Table 4 that they compete favorably with various particleboards based on lignocellulosic

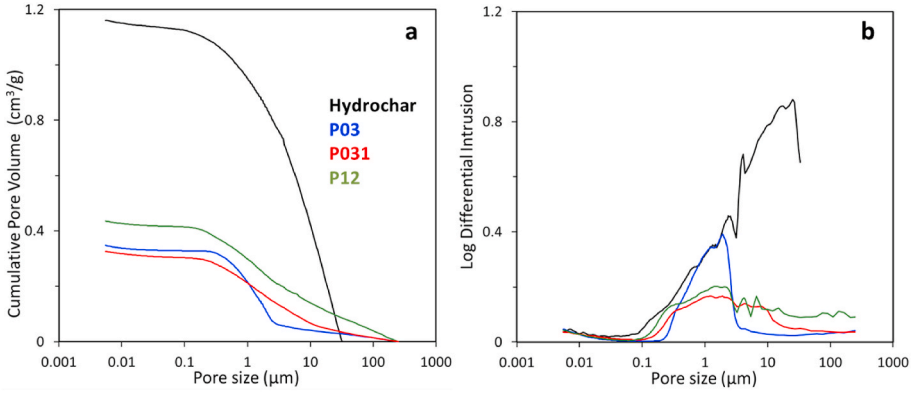

Fig. 3. Cumulative pore volume (a) and pore size distribution (b) of the OFMSW-hydrochar and the probes made of particles with different sizes.

Table 4
Comparison of the characteristics of different particleboards.

Particleboards	Particle size (mm)	Density (kg/m^3)	MOR (MPa)	Water Absorption 2h (%)	Thickness Swelling 2h (%)	Thermal conductivity (W/(m•K))	Ref.
Palm tree prunings + urea–formaldehyde resin	0.25–1	856	13.97	72	37.83	0.060	[49]
	1–2	840	19.85	54	25.22	0.055	
	2–4	819	12.68	59	32.11	0.054	
Washingtonia Palm Rachis + citric acid	<0.25	812	12.50	56	16.40	0.089	[31]
	0.25–1	779	12.01	59	22.10	0.086	
	1–2	801	7.36	88	34.40	0.082	
	2–4	778	3.71	91	38.10	0.080	
	4–8	687	2.77	99	48.60	0.079	
Kenaf + Urea Formaldehyderesins	<0.5	269–369	19.60	70	34	–	[32]
	0.5–1		15.10	77	28	–	
	1–2		17.00	65	26	–	
	>2		16.60	68	28	–	
Giant reed culms + starch	–	812–830	3.5–7.5	–	28.23–58.83	0.076–0.091	[50]
Acacia tree + polyurethane	<2	710	–	17.65	5.10	–	[51]
	2–4	693	–	22.09	6.45	–	
	>4	687	–	20.20	9.69	–	
Wood panel	–	300	–	–	–	0.070	[52]
	–	600	–	–	–	0.120	
	–	900	–	–	–	0.180	
Binderless OFMSW-hydrochar	<0.3 (P03)	838	14.44	21	8.52	0.091	This work
	0.3–1 (P031)	838	16.32	38	18.42	0.113	
	1-2 (P12)	883	21.64	43	45.90	0.132	

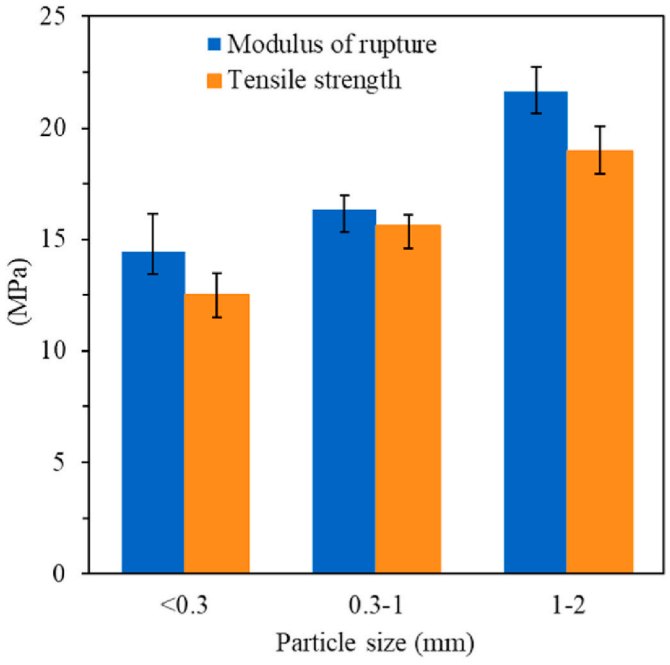

Fig. 4. Modulus of rupture and tensile strength for the different hydrochar probes.

materials that required processing with binders.

The tensile strength also increased between 12.51 and 18.99 MPa with the particle size (Fig. 4). As reported by Liu et al. [57], the high tensile strength of the probes may be the result of the formation of a strong liquid bridge linking adjacent particles. This may involve the combined action during compression of enhanced attractive forces between the functionalized surface of hydrochar particles, as well as the presence of polar organic compound residues generated by HTC and deposited on the surface of the solid by-product.

3.5. Water absorption and thickness swelling

Affinity to water is one of the main weaknesses of biomass-based particleboards since it greatly affects their dimensional stability and durability [2].

The surface oxygenated functionalities confer a hydrophilic nature to the probes, and they experience water absorption between 21 and 43 wt % after immersion in water for 2 h (Fig. 5). Table 4 shows that the hydrochar panels absorb much less water than most other samples and the highest absorption is achieved by the sample with the larger particle size (1–2 mm).

As a consequence of water absorption, the probes undergo an increase in thickness, whose degree depends greatly on the particles size (Fig. 5). Whereas the swelling in thickness accounts for 8.52% in probes with smaller particles (<0.3 mm), the use of 0.3–1 mm and 1–2 mm particles leads to expansions of 18.42% and 45.90%, respectively. The remarkable increase observed for P12 could be related to its higher pore volume (Fig. 3a) and wider PSD (Fig. 3b).

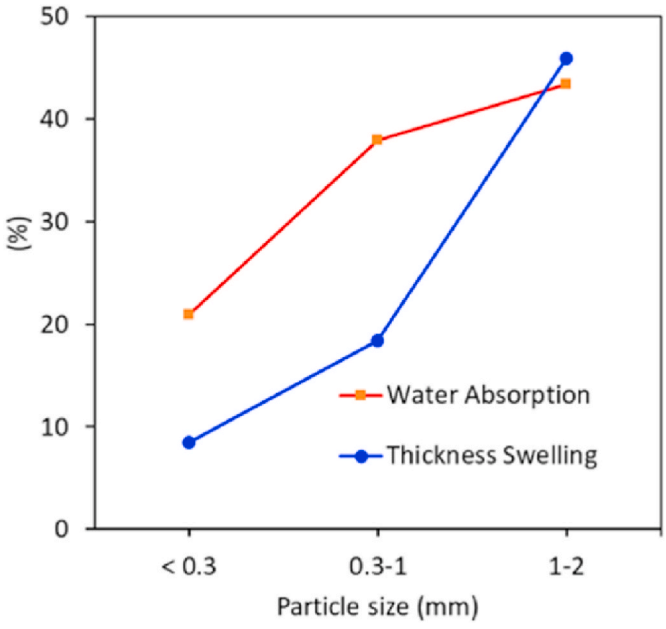

Fig. 5. Percentage of water absorption and thickness swelling after immersion of the hydrochar probes in water for 2 h.

As shown in Table 4, with the exception of P12, the present samples display lower thickness swelling than the majority of particleboards made of palm tree pruning, Washingtonia palm rachis and kenaf.

TPD experiments reveal that approximately 30% of the oxygenated groups on the P031 surface correspond to weak functionalities that desorb at temperatures below 350 °C (Fig. 2e). This suggests that the stability of the hydrochars-based particleboards against water could be improved by a simple low-temperature post-treatment to reduce the number of [O]-groups and, consequently, the material affinity to water [58,59]. Furthermore, it is very likely that with the help of water-repellent products, such as those commonly used in the wood industry, hydrochar-based panels can achieve P3 classification [52].

3.6. Thermal insulation properties and bulk density

The thermal conductivity of the OFMSW-hydrochar probes are shown in Table 4, with mean values ranging from 0.091 to 0.132 W/(m•K). The bulk density of P03 and P031 is 838 kg/m^3 and it increases to 883 kg/m^3 for P12. No linear correlation has been found between the values of bulk density and the thermal conductivity since, according to Eq. (1), the thermal diffusivity and the specific heat capacity also play a role.

At a glance, the increase of thermal conductivity with particle size seems to be related with the pores size distribution (Fig. 3b). Thus, the presence of pores larger than 4 μm in P031 and P12 appear to have a negative impact on their thermal insulating behaviour.

The low thermal conductivity of P03, comparable to the values obtained for lignocellulosic materials based-panels that are claimed as good thermal insulators in construction [31,33], suggests the potential of OFMSW-hydrochar as an alternative resource. However, improvements are still needed to meet the limiting value of 0.065 W/(m•K) set as standard for this application [60].

The significant impact of the particle size and the pores size distribution suggests that optimisation of the agglomeration process would allow upgrading the final insulation performance.

4. Conclusions

The alternative presented in this work fits into a circular economy framework based on the recovery of organic fraction of municipal solid wastes to reduce the consumption of primary resources and energy and the carbon footprint associated with panels manufacturing.

Without requiring prior drying, hydrothermal carbonization (HTC) at 180 °C for only 2 h successfully converts highly polluting wet OFMSW into a stable carbonaceous solid, the so-called hydrochar. The HTC process yields 30 wt% of hydrochar with a carbon recovery of 44 wt%, with respect to the initial OFMSW (dry basis).

A simple pressing of the OFMSW-hydrochar particles (sizes of <0.3, 0.3–1, and 1–2 mm) at 3 MPa for 7 min at room temperature (~ 25 °C) leads to binderless probes with 30% porosity. The density is 838 kg/m^3 for the samples with particle size <0.3 mm and 0.3–1 mm, whereas that with the largest particles achieves 883 kg/m^3. Great prospects of OFMSW-derived hydrochar as resource for sustainable particleboard are indicated by modulus of rupture of 14.44–21.64 MPa and tensile strength of 12.51–18.99 MPa. The use of larger particles improves the mechanical stability of the probes, but also favors water absorption and thickness swelling.

Thermal conductivity values in the range of 0.091–0.132 W/(m•K) suggest the potential of OFMSW-hydrochar for thermal insulation panels.

The reduction of water absorption and dimensional changes and the improvement of thermal insulation properties by suiting the chemical properties of the raw hydrochar and the particleboard processing (e.g., use of other production methods and additives) are being addressed in other ongoing research.

Author contributions

Michael M. Santos: Conceptualization; Formal analysis; Investigation; Methodology; Writing - original draft. Maria A. Diez: Investigation; Methodology; Resources; Supervision; Writing - review & editing. Marta Suárez: Investigation; Methodology; Writing - original draft. Teresa A. Centeno: Conceptualization; Formal analysis; Funding acquisition; Investigation; Methodology; Resources; Supervision; Writing - original draft; Writing - review & editing.

Declaration of competing interest

The authors declare that they have no known competing financial interests or personal relationships that could have appeared to influence the work reported in this paper.

Acknowledgments

Funding from the European Regional Development Fund (ERDF) through project CEMOWAS^2 (SOE2/P5/F0505)-INTERREG V SUDOE 2017 is acknowledged. Michael M. Santos thanks the University of Beira Interior and the Spanish National Research Council (CSIC) for the award of an Erasmus+ internship.

This study would not have been possible without the help of Loreto Suárez (INCAR-CSIC) and Dr. Luis Antonio Díaz (CINN-CSIC) for the hydrochar preparation and the mechanical strength tests, respectively.

The support from COGERSA SAU (company for solid waste management in Asturias, Spain) is highly appreciated.

Appendix A. Supplementary data

Supplementary data to this article can be found online at https://doi.org/10.1016/j.jobe.2021.103375.

References

[1] Z. Zhao, F. Xiao, S. Amirkhanian, Recent applications of waste solid materials in pavement engineering, Waste Manag. 108 (2020) 78–105, https://doi.org/10.1016/j.wasman.2020.04.024.

[2] M.V. Madurwar, R.V. Ralegaonkar, S.A. Mandavgane, Application of agro-waste for sustainable construction materials: a review, Construct. Build. Mater. 38 (2013) 872–878, https://doi.org/10.1016/j.conbuildmat.2012.09.011.

[3] H. Maljaee, R. Madadi, H. Paiva, L. Tarelho, V.M. Ferreira, Incorporation of biochar in cementitious materials: a roadmap of biochar selection, Construct. Build. Mater. 283 (2021), 122757, https://doi.org/10.1016/j.conbuildmat.2021.122757.

[4] Z. Tang, W. Li, V.W.Y. Tam, C. Xue, Advanced progress in recycling municipal and construction solid wastes for manufacturing sustainable construction materials, Resour. Conserv. Recycl. X. 6 (2020), 100036, https://doi.org/10.1016/j.rcrx.2020.100036.

[5] Z. Tang, W. Li, G. Ke, J.L. Zhou, V.W.Y. Tam, Sulfate attack resistance of sustainable concrete incorporating various industrial solid wastes, J. Clean. Prod. 218 (2019) 810–822, https://doi.org/10.1016/j.jclepro.2019.01.337.

[6] L.T.T. Vo, P. Navard, Treatments of plant biomass for cementitious building materials – a review, Construct. Build. Mater. 121 (2016) 161–176, https://doi.org/10.1016/j.conbuildmat.2016.05.125.

[7] F. Giglio, The use of materials from biomass as construction materials, Open J. Civ. Eng. (2013) 82–84, https://doi.org/10.4236/ojce.2013.32a009, 03.

[8] R.S.F. Martins, F.G. Gonçalves, P.G. de A. Segundinho, R.C.C. Lelis, J.B. Paes, Y. M. Lopez, I.L.S. Chaves, R.G.E. de Oliveira, Investigation of agro-industrial lignocellulosic wastes in fabrication of particleboard for construction use, J. Build. Eng. 43 (2021), 102903, https://doi.org/10.1016/j.jobe.2021.102903.

[9] R.S.F. Martins, F.G. Gonçalves, R.C.C. Lelis, P.G.A. Segundinho, A.M. Nunes, G. B. Vidaurre, I.L.S. Chaves, S.B. Santiago, Physical properties and formaldehyde emission in particleboards of Eucalyptus sp. and lingo-cellulosic agro-industrial waste, Sci. For. Sci. 48 (2020) 1–14, https://doi.org/10.18671/scifor.v48n125.13.

[10] L. Nunes, E. Cintura, J.L. Parracha, B. Fernandes, V. Silva, P. Faria, Cement-bonded particleboards with banana pseudostem waste: physical performance and biosusceptibility, Infrastructure 6 (2021) 86, https://doi.org/10.3390/infrastructures6060086.

[11] M.C. Wong, S.I.S. Hendrikse, P.C. Sherrell, A.V. Ellis, Grapevine waste in sustainable hybrid particleboard production, Waste Manag. 118 (2020) 501–509, https://doi.org/10.1016/j.wasman.2020.09.007.

[12] I. Cosentino, L. Restuccia, G.A. Ferro, J.M. Tulliani, Type of materials, pyrolysis conditions, carbon content and size dimensions: the parameters that influence the

mechanical properties of biochar cement-based composites, Theor. Appl. Fract. Mech. 103 (2019), 102261, https://doi.org/10.1016/j.tafmec.2019.102261.
[13] S. Gupta, P. Krishnan, A. Kashani, H.W. Kua, Application of biochar from coconut and wood waste to reduce shrinkage and improve physical properties of silica fume-cement mortar, Construct. Build. Mater. 262 (2020), 120688, https://doi.org/10.1016/j.conbuildmat.2020.120688.
[14] S. Muthukrishnan, S. Gupta, H.W. Kua, Application of rice husk biochar and thermally treated low silica rice husk ash to improve physical properties of cement mortar, Theor. Appl. Fract. Mech. 104 (2019), 102376, https://doi.org/10.1016/j.tafmec.2019.102376.
[15] Q. Ren, Z. Zeng, Z. Jiang, Q. Chen, Incorporation of bamboo charcoal for cement-based humidity adsorption material, Construct. Build. Mater. 215 (2019) 244–251, https://doi.org/10.1016/j.conbuildmat.2019.04.173.
[16] S. Gupta, H.W. Kua, Application of rice husk biochar as filler in cenosphere modified mortar: preparation, characterization and performance under elevated temperature, Construct. Build. Mater. 253 (2020), 119083, https://doi.org/10.1016/j.conbuildmat.2020.119083.
[17] W.M. Lewandowski, M. Ryms, W. Kosakowski, Thermal biomass conversion: a review, Processes 8 (2020), https://doi.org/10.3390/PR8050516.
[18] A.K. Sakhiya, A. Anand, P. Kaushal, Production, Activation, and Applications of Biochar in Recent Times, Springer Singapore, 2020, https://doi.org/10.1007/s42773-020-00047-1.
[19] J.A. Libra, K.S. Ro, C. Kammann, A. Funke, N.D. Berge, Y. Neubauer, M.M. Titirici, C. Fühner, O. Bens, J. Kern, K.H. Emmerich, Hydrothermal carbonization of biomass residuals: a comparative review of the chemistry, processes and applications of wet and dry pyrolysis, Biofuels 2 (2011) 71–106, https://doi.org/10.4155/bfs.10.81.
[20] M.M. Titirici, M. Antonietti, Chemistry and materials options of sustainable carbon materials made by hydrothermal carbonization, Chem. Soc. Rev. 39 (2010) 103–116, https://doi.org/10.1039/b819318p.
[21] H.S. Kambo, A. Dutta, A comparative review of biochar and hydrochar in terms of production, physico-chemical properties and applications, Renew. Sustain. Energy Rev. 45 (2015) 359–378, https://doi.org/10.1016/j.rser.2015.01.050.
[22] Z. Zhang, J. Yang, J. Qian, Y. Zhao, T. Wang, Y. Zhai, Biowaste hydrothermal carbonization for hydrochar valorization: skeleton structure, conversion pathways and clean biofuel applications, Bioresour. Technol. 324 (2021), 124686, https://doi.org/10.1016/j.biortech.2021.124686.
[23] N.U. Saqib, H.B. Sharma, S. Baroutian, B. Dubey, A.K. Sarmah, Valorisation of food waste via hydrothermal carbonisation and techno-economic feasibility assessment, Sci. Total Environ. 690 (2019) 261–276, https://doi.org/10.1016/j.scitotenv.2019.06.484.
[24] M.-M. Fu, C.-H. Mo, H. Li, Y.-N. Zhang, W.-X. Huang, M.H. Wong, Comparison of physicochemical properties of biochars and hydrochars produced from food wastes, J. Clean. Prod. 236 (2019), 117637, https://doi.org/10.1016/j.jclepro.2019.117637.
[25] M. Lucian, M. Volpe, F. Merzari, D. Wüst, A. Kruse, G. Andreottola, L. Fiori, Hydrothermal carbonization coupled with anaerobic digestion for the valorization of the organic fraction of municipal solid waste, Bioresour. Technol. 314 (2020), 123734, https://doi.org/10.1016/j.biortech.2020.123734.
[26] M. Lucian, M. Volpe, L. Gao, G. Piro, J.L. Goldfarb, L. Fiori, Impact of hydrothermal carbonization conditions on the formation of hydrochars and secondary chars from the organic fraction of municipal solid waste, Fuel 233 (2018) 257–268, https://doi.org/10.1016/j.fuel.2018.06.060.
[27] B. Motavaf, R.A. Dean, J. Nicolas, P.E. Savage, Hydrothermal carbonization of simulated food waste for recovery of fatty acids and nutrients, Bioresour. Technol. (2021), 125872, https://doi.org/10.1016/j.biortech.2021.125872.
[28] ASTM D7582 - 15, Standard Test Methods for Proximate Analysis of Coal and Coke by Macro Thermogravimetric Analysis.
[29] ISO 18123, Solid Biofuels. Determination of the Content of Volatile Matter, 2015, 2015.
[30] T. Wang, Y. Zhai, Y. Zhu, C. Li, G. Zeng, A review of the hydrothermal carbonization of biomass waste for hydrochar formation: process conditions, fundamentals, and physicochemical properties, Renew. Sustain. Energy Rev. 90 (2018) 223–247, https://doi.org/10.1016/j.rser.2018.03.071.
[31] M.T. Ferrandez-Garcia, A. Ferrandez-Garcia, T. Garcia-Ortuño, C.E. Ferrandez-Garcia, M. Ferrandez-Villena, Influence of particle size on the properties of boards made from Washingtonia palm rachis with citric acid, Sustain. Times 12 (2020) 4841, https://doi.org/10.3390/SU12124841.
[32] A.H. Juliana, M.T. Paridah, Evaluation of basic properties of kenaf (Hibiscus cannabinus L.) particles as raw material for particleboard, ICCM Int. Conf. Compos. Mater. 36 (2011) 1–6.
[33] A. Laborel-Préneron, C. Magniont, J.E. Aubert, Characterization of barley straw, hemp shiv and corn cob as resources for bioaggregate based building materials, Waste and Biomass Valorization 9 (2018) 1095–1112, https://doi.org/10.1007/s12649-017-9895-z.
[34] Y. Lin, X. Ma, X. Peng, Z. Yu, S. Fang, Y. Lin, Y. Fan, Combustion, pyrolysis and char CO2-gasification characteristics of hydrothermal carbonization solid fuel from municipal solid wastes, Fuel 181 (2016) 905–915, https://doi.org/10.1016/j.fuel.2016.05.031.
[35] X. Chen, X. Ma, X. Peng, Y. Lin, Z. Yao, Conversion of sweet potato waste to solid fuel via hydrothermal carbonization, Bioresour. Technol. 249 (2018) 900–907, https://doi.org/10.1016/j.biortech.2017.10.096.
[36] H.B. Sharma, B.K. Dubey, Binderless fuel pellets from hydrothermal carbonization of municipal yard waste: effect of severity factor on the hydrochar pellets properties, J. Clean. Prod. 277 (2020), 124295, https://doi.org/10.1016/j.jclepro.2020.124295.
[37] UNE-EN317:1994, Particleboards and Fibreboards - Determination of Swelling in Thickness after Immersion in Water, 1994.
[38] W.J. Parker, R.J. Jenkins, C.P. Butler, G.L. Abbott, Flash method of determining thermal diffusivity, heat capacity, and thermal conductivity, J. Appl. Phys. 32 (1961), 1679, https://doi.org/10.1063/1.1728417.
[39] UNE-EN 323, Tableros derivados de la madera, Determinacion de la densidad, 1994.
[40] R. Campuzano, S. González-Martínez, Characteristics of the organic fraction of municipal solid waste and methane production: a review, Waste Manag. 54 (2016) 3–12, https://doi.org/10.1016/j.wasman.2016.05.016.
[41] J.A. Pajares, M.A. Díez, Coal and coke, in: J. Reedijk, M. Waltham (Eds.), Elsevier Ref. Modul. Chem. Mol. Sci. Chem. Eng., Elsevier, 2014, https://doi.org/10.1016/B978-0-12-409547-2.10968-0.
[42] I. Suárez-Ruiz, M. Diez, F. Rubiera, Coal, in: I. Suárez-Ruiz, M. Diez, F. Rubiera (Eds.), New Trends Coal Conversion, WoodHead Publishing. Elsevier, 2019, p. 6.
[43] H. Bhakta Sharma, S. Panigrahi, B.K. Dubey, Food waste hydrothermal carbonization: study on the effects of reaction severities, pelletization and framework development using approaches of the circular economy, Bioresour. Technol. 333 (2021), 125187, https://doi.org/10.1016/j.biortech.2021.125187.
[44] M.A. Diez, R. Alvarez, M. Fernández, Biomass derived products as modifiers of the rheological properties of coking coals, Fuel 96 (2012) 306–313, https://doi.org/10.1016/j.fuel.2011.12.065.
[45] J. Figueiredo, M.F. Pereira, M.M. Freitas, J.J. Órfão, Modification of the surface chemistry of activated carbons, Carbon N. Y. 37 (1999) 1379–1389, https://doi.org/10.1016/S0008-6223(98)00333-9.
[46] G.S. Szymański, Z. Karpiński, S. Biniak, A. Świątkowski, The effect of the gradual thermal decomposition of surface oxygen species on the chemical and catalytic properties of oxidized activated carbon, Carbon 40 (2002) 2627–2639, https://doi.org/10.1016/S0008-6223(02)00188-4.
[47] ANSI-A208-1-1999-Particleboard, ANSI-A208-1-1999-Particleboard.
[48] M.T. Reza, J.G. Lynam, V.R. Vasquez, C.J. Coronella, Pelletization of biochar from hydrothermally carbonized wood, Environ. Prog. Sustain. Energy 31 (2012) 225–234.
[49] C.E. Ferrández-García, A. Ferrández-García, M. Ferrández-Villena, J.F. Hidalgo-Cordero, T. García-Ortuño, M.T. Ferrández-García, Physical and mechanical properties of particleboard made from palm tree prunings, Forests 9 (2018) 1–14, https://doi.org/10.3390/f9120755.
[50] C.E. Ferrández-García, J. Andreu-Rodríguez, M.T. Ferŕndez-García, M. Ferŕndez-Villena, T. García-Ortuño, Panels made from giant reed bonded with non-modified starches, BioResources 7 (2012) 5904–5916, https://doi.org/10.15376/biores.7.4.5904-5916.
[51] M.N.M. Baharuddin, N.M. Zain, E.N. Roslin, W.S.W. Harun, Zaeime, Physical properties of homogeneous particleboard based on acacia tree and polyurethane adhesive as a resins, Int. J. Eng. Adv. Technol. 8 (2019) 3382–3387, https://doi.org/10.35940/ijeat.F9506.088619.
[52] 2015 UNE-EN 13986:2006+A1, Wood-based Panels for Use in Construction - Characteristics, Evaluation of Conformity and Marking, 2015.
[53] G. Nemli, S. Demirel, Relationship between the density profile and the technological properties of the particleboard composite, J. Compos. Mater. 41 (2007) 1793–1802, https://doi.org/10.1177/0021998307069892.
[54] S. Hegazy, K. Ahmed, Effect of date palm cultivar, particle size, panel density and hot water extraction on particleboards manufactured from date palm fronds, Agriculture 5 (2015) 267–285, https://doi.org/10.3390/agriculture5020267.
[55] M.T. Ferrandez-García, A. Ferrandez-Garcia, T. Garcia-Ortuño, C.E. Ferrandez-Garcia, M. Ferrandez-Villena, Assessment of the physical, mechanical and acoustic properties of Arundo donax L. biomass in low pressure and temperature particleboards, Polymers (Basel) 12 (2020) 1361, https://doi.org/10.3390/POLYM12061361.
[56] A. Prokop, R.K. Bajpai, M.E. Zappi, Utilization Alternatives of Algal Wastes for Solid Algal Products, Algal Biorefineries 2 (2015) 1–557, https://doi.org/10.1007/978-3-319-20200-6.
[57] Z. Liu, A. Quek, R. Balasubramanian, Preparation and characterization of fuel pellets from woody biomass, agro-residues and their corresponding hydrochars, Appl. Energy 113 (2014) 1315–1322, https://doi.org/10.1016/j.apenergy.2013.08.087.
[58] H.F. Stoeckli, F. Kraehenbuehl, D. Morel, The adsorption of water by active carbons, in relation to the enthalpy of immersion, Carbon 21 (1983) 589–591, https://doi.org/10.1016/0008-6223(83)90243-9.
[59] F. Carrasco-Marin, A. Mueden, T.A. Centeno, F. Stoeckli, C. Moreno-Castilla, Water adsorption on activated carbons with different degrees of oxidation, J. Chem. Soc. Faraday. Trans. 93 (1997) 2211–2215.
[60] L. Matias, P. dos Santos, Coeficientes de transmissão térmica de elementos da envolvente dos edifícios ITE 50, LNEC - laboratório Nac, Eng. Civi. (2009).